J|A|C|S
ARTICLES
Published on Web 12/20/2007

Reactivity of Hydrogen with Solid-State Films of Alkylamine- and Tetraoctylammonium Bromide-Stabilized Pd, PdAg, and PdAu Nanoparticles for Sensing and Catalysis Applications

Francisco J. Ibañez and Francis P. Zamborini*

Department of Chemistry, University of Louisville, Louisville, Kentucky 40292

Received August 9, 2007; E-mail: f.zamborini@louisville.edu

Abstract: Hydrogen gas spontaneously adsorbs to Pd metal as atomic hydrogen and diffuses into the lattice to form PdH_x. We previously showed that films of hexanethiolate-coated Pd monolayer-protected clusters (MPCs) do not readily react with H_2 due to the strong chemical bonding of the thiolate to the Pd, which inhibits the reaction. Consequently, these films require ozone or heat treatment for reactivity to occur, which is inconvenient for sensing or catalysis applications. In this report, we describe the reactivity between H_2 and solid-state films of alkylamine-coated Pd, PdAg (10:1), and PdAu (10:1) MPCs and films of tetraoctylammonium bromide (TOABr)-stabilized Pd and PdAg (10:1) nanoparticles as determined by changes in film conductivity. Our data show that Pd nanoparticles coated with these more weakly coordinated amine or ammonium groups readily react with H_2 without any need for ozone or heat treatment. The conductivity of films of octylamine ($C8NH_2$)- or dodecylamine ($C12NH_2$)-coated Pd, PdAg, and PdAu MPCs increases irreversibly upon initial exposure to 100% H_2 to varying degrees and with different reaction kinetics and then exhibits stable, reversible changes in the presence of H_2 concentrations ranging from 9.6 to 0.08%. The behavior upon initial exposure to H_2 (conditioning) and the direction and magnitude of the reversible conductivity changes depend on the alkyl chainlength and alloy composition. Films of TOABr-coated Pd and PdAg nanoparticles show stable, reversible increases in conductivity in the presence of H_2 concentrations from 9.6 down to 0.11% without conditioning. Surface FTIR spectroscopy and atomic force microscopy (AFM) provide information about the organic monolayer and film morphology, respectively, following reactivity with H_2. This work demonstrates a simple approach toward preparing films of chemically synthesized Pd-containing nanoparticles with controlled reactivity to H_2 for sensing and catalysis applications.

Introduction

The reaction between hydrogen and Pd or Pd-containing alloys is of great interest because of its relevance in H_2 sensing and heterogeneous and homogeneous catalysis. It is well known that H_2 spontaneously adsorbs to Pd as atomic H and diffuses into the lattice to form PdH_x.[1] The initial α-phase Pd becomes β-phase PdH_x through an $\alpha-\beta$ phase transition. The Pd lattice spacing changes throughout these phase changes, depending on the H_2 concentration[1,2] in the surrounding atmosphere. The phase transitions and changes in lattice spacing lead to measurable changes in the optical properties,[3−11] resistance,[12−32] and mass[2,8] of the Pd, which has been heavily exploited for H_2 sensing. Palladium's ability to break and adsorb H has also led to its use for catalyzing various reactions.

H_2 is a useful energy source that has the potential to reduce the need for fossil fuels in the future. A great deal of effort has

(1) Lewis, F. A. *The Palladium/Hydrogen System*; Academic Press Inc.: London, 1967.
(2) Christofides, C.; Mandelis, A. *J. Appl. Phys.* **1990**, *68*, 1−30.
(3) Bévenot, X.; Trouillet, A.; Veillas, C.; Gagnaire, H.; Clément, M. *Sens. Actuators, B* **2000**, *67*, 57−67.
(4) Garcia, J. A.; Mandelis, A. *Rev. Sci. Instrum.* **1996**, *67*, 3981−3983.
(5) Kalli, K.; Othonos, A.; Christofides, C. *Rev. Sci. Instrum.* **1998**, *69*, 3331−3338.
(6) Kalli, K.; Othonos, A.; Christofides, C. *J. Appl. Phys.* **2002**, *91*, 3829−3840.
(7) Lin, H.; Gao, T.; Fantini, J.; Sailor, M. J. *Langmuir* **2004**, *20*, 5104−5108.
(8) Smith, A. L.; Shirazi, H. M. *Thermochim. Acta* **2005**, *432*, 202−211.
(9) Zhao, Z.; Carpenter, M. A. *J. Appl. Phys.* **2005**, *97*, 124301.
(10) Zhao, Z.; Carpenter, M. A.; Xia, H.; Welch, D. *Sens. Actuators, B* **2006**, *113*, 532−538.
(11) Zhao, Z.; Sevryugina, Y.; Carpenter, M. A.; Welch, D.; Xia, H. *Anal. Chem.* **2004**, *76*, 6321−6326.
(12) Dankert, O.; Pundt, A. *Appl. Phys. Lett.* **2002**, *81*, 1618−1620.
(13) Dwivedi, D.; Dwivedi, R.; Srivastava, S. K. *Sens. Actuators, B* **2000**, *71*, 161−168.
(14) Favier, F.; Walter, E. C.; Zach, M. P.; Benter, T.; Penner, R. M. *Science* **2001**, *293*, 2227−2231.
(15) Huang, L.; Gong, H.; Peng, D.; Meng, G. *Thin Solid Films* **1999**, *345*, 217−221.
(16) Hughes, R. C.; Schubert, W. K. *J. Appl. Phys.* **1992**, *71*, 542−544.
(17) Hughes, R. C.; Schubert, W. K.; Zipperian, T. E.; Rodriguez, J. L.; Plut, T. A. *J. Appl. Phys.* **1987**, *62*, 1074−1083.
(18) Kaltenpoth, G.; Schnabel, P.; Menke, E.; Walter, E. C.; Grunze, M.; Penner, R. M. *Anal. Chem.* **2003**, *75*, 4756−4765.
(19) Kang, W. P.; Gürbüz, Y. *J. Appl. Phys.* **1994**, *75*, 8175−8181.
(20) Kolmakov, A.; Klenov, D. O.; Lilach, Y.; Stemmer, S.; Moskovits, M. *Nano Lett.* **2005**, *5*, 667−673.
(21) Kong, J.; Chapline, M. G.; Dai, H. *Adv. Mater.* **2001**, *13*, 1384−1386.
(22) Luongo, K.; Sine, A.; Bhansali, S. *Sens. Actuators, B* **2005**, *111−112*, 125−129.
(23) Lutz, B. J.; Fan, Z. H. *Anal. Chem.* **2005**, *77*, 4969−4975.
(24) Mizsei, J.; Voutilainen, J.; Saukko, S.; Lantto, V. *Thin Solid Films* **2001**, *391*, 209−215.
(25) Morris, J. E.; Kiesow, A.; Hong, M.; Wu, F. *Int. J. Electron.* **1996**, *81*, 441−447.
(26) Sakamoto, Y.; Takai, K.; Takashima, I.; Imada, M. *J. Phys.: Condens. Matter* **1996**, *8*, 3399−3411.
(27) Sayago, I.; Terrado, E.; Lafuente, E.; Horrillo, M. C.; Maser, W. K.; Benito, A. M.; Navarro, R.; Urriolabeitia, E. P.; Martinez, M. T.; Gutierrez, J. *Synth. Met.* **2005**, *148*, 15−19.

10.1021/ja076000h CCC: $40.75

been put forth to develop H_2-fueled motor vehicles to fulfill increasing energy demands for transportation. Also, H_2 is present as a common reagent in industry and used as an O_2 scavenger in metallurgy, in hydrocracking for refined fuels, and in degradation of synthetic materials.[33] Operating with H_2 can be dangerous because it is explosive in air above 4%.[2] Accordingly, one of the aims in fuel cell[34] research and other applications is to safely store[35,36] and release H_2 in a controlled manner. For these reasons, it is important to develop simple, reliable, low-cost sensors for the detection of H_2 over a range of concentrations.

In the area of catalysis, there is an increasing interest in the use of chemically synthesized, reusable metal nanoparticles to catalyze reactions with large turnover rates and high selectivity. Organic stabilizers have the critical role of providing size and shape control and reduced size dispersity during synthesis. They also provide stability by preventing nanoparticle aggregation and size and shape changes during the catalytic reaction. While serving these functions, the stabilizer should also prevent poisoning of the catalyst and not deter the reactivity of the metal nanoparticle itself. Chemically synthesized catalyst particles can often be easily separated from the reaction products and reused. Crooks and co-workers recently demonstrated the use of dendrimer-encapsulated Pd nanoparticles for catalyzing the hydrogenation of olefins.[37] Others catalyzed the transformation of aromatic nitro and azide compounds to their corresponding amines by the reaction with Pd nanoparticles attached to ferrite nanoparticles through amine groups, where the catalyst could be easily separated magnetically via the ferrite nanoparticles.[38] Other examples include thioether-,[39] tetraoctylammonium bromide (TOABr)-,[40] and chalcogenide-stabilized Pd nanoparticles in the presence of thiols[41] for the hydrogenation of 6-bromo-1-hexane, styrene, and various alkynes, respectively. Thiol-stabilized Pt nanoparticles[42] and binol-functionalized Au nanoparticles[43] have also served as catalysts for the hydrogenation of allyl alcohol and benzaldehyde, respectively. There have been no previous studies to our knowledge on the reactivity of alkylamine-stabilized Pd nanoparticles with H_2 for sensing or catalysis and no study on TOABr-coated Pd nanoparticles for H_2 sensing.

Early chemiresistive H_2 sensors reported in the literature were based on conductive Pd films whose resistance increased in the presence of hydrogen due to the formation of the more resistive PdH_x.[1,26] More recent reports on this type of sensing mechanism demonstrated improved response times, higher sensitivity, and lower detection limits by using nanostructured materials (Pd nanotubes).[31] Another type of sensing mechanism involves the use of Pd nanowires[14,28] or films of nanoparticles[12,30] that contain disconnected, high resistance metal−metal junctions. These materials exhibit a decrease in resistance in the presence of H_2 due to the formation of PdH_x, which expands in volume and forms a more connected, lower resistance structure. Penner and co-workers demonstrated this behavior with Pd mesowires electrochemically synthesized by step-edge decoration of highly oriented pyrolytic graphite (HOPG)[14,28,32] and lithographically fabricated Pd wires.[18,44] Others have described similar behavior for discontinuous films of Pd, which contain Pd nanoparticles evaporated or sputtered so that they are below the percolation threshold for conductivity.[12,22,25,30] Zach and co-workers demonstrated the importance of the functionality of the substrate that the Pd is deposited on.[30] In general, these types of sensors exhibit very fast, reversible, and sensitive responses with detection limits as low as 0.05 ppm and response times on the order of milliseconds.[14,30]

We previously described the reactivity of hexanethiolate-coated Pd monolayer-protected clusters (MPCs) to H_2 for chemiresistive sensing applications.[45] This was the first report on films of chemically synthesized Pd nanoparticles for H_2 sensing, which has several potential benefits over evaporated or sputtered Pd films in terms of simplicity, cost, reproducibility, and control over the electronic properties and sensing behavior. Although the electronic properties of Pd MPCs can be tailored by the surrounding monolayer, the presence of the strongly chemisorbed thiolate group prevented the reaction between Pd and H_2. This required ozone or heat treatment to desorb thiolates from the surface and promote H_2 reactivity, which is inconvenient and more complicated. It would be beneficial to synthesize Pd nanoparticles that could be deposited as a film and directly utilized for H_2 sensing and catalysis without treatment. Here we report the reactivity of solid-state films containing alkylamine-[46] and tetraoctylammonium bromide (TOABr)-coated Pd,[40] PdAg, and PdAu alloys with H_2 as determined by changes in conductivity as well as surface reflectance FTIR spectroscopy and atomic force microscopy (AFM) measurements on the films. Importantly, we find that the alkylamine and ammonium-containing molecules stabilize the Pd nanoparticles but do not inhibit their reactivity with H_2, as in the case of hexanethiolates. We describe the details of the reactivity as a function of alkyl chainlength, type of ligand (amine or ammonium), and metal composition.

Experimental Section

Chemicals. Sodium borohydride (99%), tetraoctylammonium bromide (99%), toluene (99.9%), 2-propanol (99.9%), ethanol (200 proof), dichloromethane (99%), and acetonitrile (99%) were purchased from VWR Scientific Products. Hexanethiol (C6S), octylamine ($C_8H_{25}NH_2$),

(28) Walter, E. C.; Favier, F.; Penner, R. M. *Anal. Chem.* **2002**, *74*, 1546−1553.
(29) Wolfe, D. B.; Love, J. C.; Paul, K. E.; Chabinyc, M. L.; Whitesides, G. M. *Appl. Phys. Lett.* **2002**, *80*, 2222−2224.
(30) Xu, T.; Zach, M. P.; Xiao, Z. L.; Rosenmann, D.; Welp, U.; Kwok, W. K.; Crabtree, G. W. *Appl. Phys. Lett.* **2005**, *86*, 203104.
(31) Yu, S.; Welp, U.; Hua, L. Z.; Rydh, A.; Kwok, W. K.; Wang, H. H. *Chem. Mater.* **2005**, *17*, 3445−3450.
(32) Yun, M.; Myung, N. V.; Vasquez, R. P.; Lee, C.; Menke, E.; Penner, R. M. *Nano Lett.* **2004**, *4*, 419−422.
(33) Ramachandran, R.; Menon, R. K. *Int. J. Hydrogen Energy* **1998**, *23*, 593−598.
(34) Che, G.; Lakshmi, B. B.; Fisher, E. R.; Martin, C. R. *Nature* **1998**, *393*, 346−349.
(35) Schalpbach, L.; Zuttel, A. *Nature* **2001**, *414*, 353−358.
(36) Horonouchi, S.; Yamanoi, Y.; Yonezawa, T.; Mouri, T.; Nishihara, H. *Langmuir* **2006**, *22*, 1880−1884.
(37) Niu, Y.; Yeung, L. K.; Crooks, R. M. *J. Am. Chem. Soc.* **2001**, *123*, 6840−6846.
(38) Guin, D.; Baruwati, B.; Manorama, S. V. *Org. Lett.* **2007**, *9*, 1419−1421.
(39) Ganesan, M.; Freemantle, R. G.; Obare, S. O. *Chem. Mater.* **2007**.
(40) Hwang, C.-B.; Fu, Y.-S.; Lu, Y.-L.; Jang, S.-W.; Chou, P.-T.; Wang, C. R. C.; Yu, S.-J. *J. Catal.* **2000**, *195*, 336−341.
(41) Ananikov, V. P.; Orlov, N. V.; Beletskaya, I. P.; Khrustalev, V. N.; Antipin, M. Y.; Timofeeva, T. V. *J. Am. Chem. Soc.* **2007**, *129*, 7252−7253.
(42) Eklund, S. E.; Cliffel, D. E. *Langmuir* **2004**, *20*, 6012−6018.
(43) Marubayashi, K.; Takizawa, S.; Kawakuzu, T.; Arai, T.; Sasai, H. *Org. Lett.* **2003**, *5*, 4409−4412.
(44) Im, Y.; Lee, C.; Vazquez, R. P.; Bangar, M. A.; Myung, N. V.; Menke, E. J.; Penner, R. M.; Yun, M. *Small* **2006**, *2*, 356−358.
(45) Ibañez, F. J.; Zamborini, F. P. *Langmuir* **2006**, *22*, 9789−9796.
(46) Kumar, A.; Mandal, S.; Selvakannan, P. R.; Pasricha, R.; Mandale, A. B.; Sastry, M. *Langmuir* **2003**, *19*, 6277−6282.

dodecylamine ($C_{12}H_{25}NH_2$), K_2PdCl_4, and $AgC_2F_3O_2$ were purchased from Aldrich Chemical Co. 1-hexadecylamine ($C_{16}H_{36}NH_2$) containing $C_{18}H_{37}NH_2$ and 1-octadecylamine ($C_{18}H_{37}NH_2$) were purchased from Alfa Aesar Co. $HAuCl_4 \cdot 3\ H_2O$ was synthesized from metallic Au. Barnstead Nanopure water (17.8 MΩ-cm) was employed for all aqueous solutions.

Synthesis of Hexanethiolate-Coated Pd MPCs. Hexanethiolate-coated (C6S) Pd monolayer-protected clusters (MPCs) were synthesized according to a modified Brust reaction[47] as reported previously.[45,48] Briefly, 0.40 g of K_2PdCl_4 was dissolved in 25 mL of water, and 1.00 g of tetraoctylammonium bromide (TOABr) was dissolved in 150 mL of toluene. The two solutions were combined and stirred until all of the $PdCl_4^{2-}$ transferred into the toluene phase. The toluene phase was separated, and 90 μL of hexanethiol, corresponding to a 1:2 thiol/Pd ratio, was added to the toluene and stirred. The solution was cooled to ~0 °C using an ice bath and a 10-fold excess of $NaBH_4$ (0.46 g in 10 mL of water) with respect to Pd was added to the toluene solution with stirring. The solution turned black within a few seconds, indicating the formation of metallic Pd MPCs. Ten milliliters of additional water was added, and the solution was stirred overnight. The toluene layer was separated and removed by rotary evaporation. The remaining black solid was suspended in 200 mL of acetonitrile and collected by filtration on a glass fritted Büchner funnel. The black solid product was washed with an additional 250 mL of acetonitrile and thoroughly dried before collecting. The average diameter of Pd MPCs prepared this way is 3.0 nm according to literature.[48]

Synthesis of Alkylamine-Coated Pd, PdAg, and PdAu MPCs. Alkylamine-coated Pd MPCs were synthesized similar to previously reported alkylamine-coated Au MPCs.[49] Solutions of 0.50 g (1.59 mmol) of K_2PdCl_4 dissolved in 20 mL of water and 1.92 g (3.51 mmol) of TOABr dissolved in 100 mL of toluene were combined and stirred until all $PdCl_4^{2-}$ transferred into the toluene phase. The appropriate alkylamine ligand was then added in a 12:1 alkylamine/Pd ratio and rapidly stirred for ~2 h. This ratio corresponds to 0.019 mol of alkylamine, which is 3.10 mL for octylamine ($C8NH_2$), 3.39 g for dodecylamine ($C12NH_2$), and 4.42 g for 1-hexadecylamine containing 1-octadecylamine ($C16\text{-}18NH_2$). The aqueous layer became cloudy white upon addition of the alkylamine due to complexation between the protonated amine and the $PdCl_4^{2-}$.[49] Next, 0.84 g of $NaBH_4$ (0.022 mol) dissolved in 10 mL of water was added to the two-phase solution while stirring. The solution turned black within a few seconds, indicating the formation of metallic Pd MPCs. Ten milliliters of additional water was added, and the solution was stirred overnight. The toluene layer was separated and removed by rotary evaporation. The remaining black solid was suspended in 200 mL of acetonitrile, collected by filtration on a glass fritted Büchner funnel, and washed with an additional 150 mL of acetonitrile and 150 mL of ethanol before thoroughly drying and collecting. The average diameter of $C8NH_2$ Pd MPCs was 3.0 ± 0.8 nm as determined by atomic force microscopy (AFM) measurements.

Alkylamine-coated PdAg and PdAu alloy MPCs were synthesized in a 10:1 Pd:Ag or Pd:Au ratio by adding the appropriate amount of K_2PdCl_4 and $AgC_2F_3O_2$ or $HAuCl_4 \cdot 3H_2O$ salts. $AgC_2F_3O_2$ was directly soluble in the toluene phase whereas $AuCl_4^-$ was phase transferred into toluene with TOABr. The amount of alkylamine and $NaBH_4$ was 12:1 and 15:1 with respect to total metal content. Nuclear magnetic resonance (NMR) and UV−vis spectroscopy measurements on Pd, PdAg, and PdAu MPCs were consistent with the successful synthesis of pure MPCs.

Synthesis of TOABr-Coated Pd and PdAg Nanoparticles. TOABr coated Pd nanoparticles were synthesized in an identical manner as the C6S Pd MPCs, except the hexanethiol was not added. These nanoparticles are insoluble when isolated as a powder.[50] Thus, after reduction and separation from the water phase, the toluene solution was reduced to ~50 mL by rotary evaporation, filtered with a microdisc filter (acrodisc, 2 μm PTFE membrane) to remove insolubles, and then used from solution. TOABr PdAg nanoparticles were synthesized by adding $AgC_2F_3O_2$ to the solution in a final 10:1 Pd:Ag molar ratio and performing the rest of the synthesis the same as that for pure Pd. The 10-fold excess of $NaBH_4$ was with respect to the total metal. The average diameter of TOABr Pd nanoparticles was 7.0 ± 0.5 nm as determined by AFM measurements, and UV−vis spectra were consistent with the formation of metal nanoparticles.

Sensor Device. Two Au electrodes separated by 23 μm were fabricated in a clean room by standard photolithography, sputtering, and lift-off procedures on a Si/SiO_x substrate. The 100 nm thick Au electrodes were sputtered over a 10 Å thick Cr adhesion layer during the process. Wire leads were attached to the Au electrodes with Ag epoxy (cured 12 h, 80 °C), which was further insulated with an overlayer of Torr-seal epoxy (cured 12 h, 80 °C). The electrode was cleaned by rinsing in acetonitrile, dichloromethane, acetone, ethanol, and 2-propanol before drying under N_2. The device was then placed in a UVO ozone cleaner (Jelight Company Inc., Irvine, CA) for 10 min before depositing the films of nanoparticles over the electrodes. Films of alkylamine-coated MPCs were drop-cast deposited using 1−3 drops of a 4−70 mg/mL toluene solution, which leads to many multilayers of nanoparticles with film thicknesses well above the thickness of the electrodes (>100 nm). Previous transmission electron microscopy (TEM) studies show that monolayer films are hexagonally close-packed with the alkyl chains interdigitated[51] and detailed conductivity studies model the films as being well-ordered and hexagonally close-packed or packed in a cubic lattice with reasonable results.[52] The concentration and number of drops were chosen to obtain current through the film above the baseline current. Films of TOABr-coated nanoparticles were drop-cast deposited using 2 drops of an approximately 3.0 mg/mL toluene solution, which is the concentration in terms of Pd when reducing the volume to 50 mL by rotary evaporation. The concentration used to prepare the films generally increased with increasing chainlength on the Pd MPCs. The range of concentrations used leads to different film thicknesses; however, the amount deposited in all cases is enough to completely cover the two electrodes and data from a few selected samples (C6S Pd and $C8NH_2$ PdAg) showed that the sensing response was not statistically different over a small thickness range.

Gas-Sensing Experiments. Gas-sensing experiments were performed with a CH Instruments 660A (Austin, TX) electrochemical workstation operating in chronoamperometry mode. The current was monitored with time while a −0.3 V potential was applied between the two electrodes and the sample was exposed to alternating flow of pure N_2 or air and different concentrations of H_2 in the N_2 or air carrier gas. A range of H_2 concentrations was obtained using a set of flow meters (Cole Parmer, 2% error at full scale) located between the sample and gas cylinders and operated by a 3-way valve, which allows a constant H_2 flow during mixing with N_2 and avoids overpressures and artificial current spikes during sensing. The different concentrations of H_2 and the total flow rates ($H_2 + N_2$/air) used are as follows: 9.6 ± 0.3% (3.1 ± 0.1 L.min^{-1}), 6.2 ± 0.2% (4.9 ± 0.1 L.min^{-1}), 3.2 ± 0.1% (4.7 ± 0.1 L.min^{-1}), 1.0 ± 0.1% (4.7 ± 0.1 L.min^{-1}), 0.50 ± 0.02% (4.6 ± 0.1 L.min^{-1}), 0.21 ± 0.02% (4.6 ± 0.1 L.min^{-1}), 0.11 ± 0.02% (4.6 ± 0.1 L.min^{-1}), 0.08 ± 0.02% (4.6 ± 0.1 L.min^{-1}).

Characterization. Films of alkylamine- and TOABr-coated Pd and Pd alloy nanoparticles were drop-cast deposited onto Si(100)/TiW(50

(47) Brust, M.; Walker, M.; Bethell, D.; Schiffrin, D. J.; Whyman, R. *Chem. Comm.* **1994**, *7*, 801−802.
(48) Zamborini, F. P.; Gross, S. M.; Murray, R. W. *Langmuir* **2001**, *17*, 481−487.
(49) Leff, D. V.; Brandt, L.; Heath, J. R. *Langmuir* **1996**, *12*, 4723−4730.
(50) Isaacs, S. R.; Culter, E. C.; Park, J.-S.; Lee, T. R.; Shon, Y.-S. *Langmuir* **2005**, *21*, 5689−5692.
(51) Wuelfing, W. P.; Green, S. J.; Pietron, J. J.; Cliffel, D. E.; Murray, R. W. *J. Am. Chem. Soc.* **2000**, *122*, 11465−11472.
(52) Zamborini, F. P.; Smart, L.; Leopold, M. C.; Murray, R. W. *Anal. Chim. Acta* **2003**, *496*, 3−16.

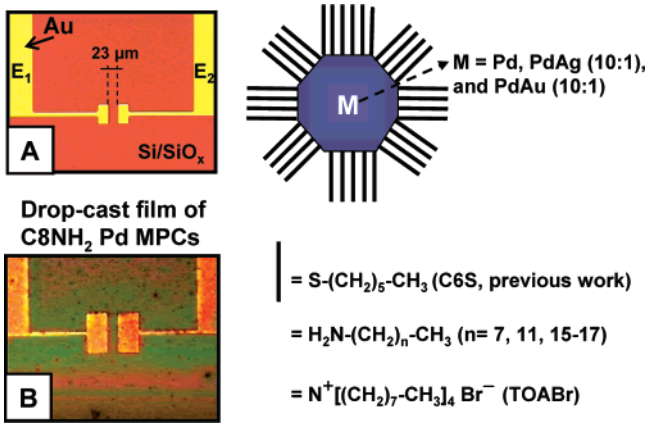

Figure 1. Optical microscope images of the electrode device (A) before and (B) after drop-cast deposition of a film of $C8NH_2$ Pd MPCs between the 23 μm electrode gap. The scheme of the nanoparticle shows the different metal compositions and different ligand stabilizers used in our previous work (C6S Pd MPCs) and this report (alkylamine- and TOABr-coated Pd and Pd alloy nanoparticles).

Å)/Au(2000 Å) and electrode devices for surface reflectance Fourier Transform Infrared (FTIR) spectroscopy and AFM experiments, respectively. FTIR data were acquired using a Digilab FTS 7000 spectrometer (Varian, Cambridge, MA) in reflectance mode with a liquid N_2-cooled MCT detector. AFM images were acquired with a Veeco Digital Instruments Nanoscope 3A Multimode Scanning Probe Microscope (Santa Barbara, CA) using a Si tip operating in tapping mode. ^{1}H Proton NMR and UV−vis spectroscopy were obtained with an INOVA 500 MHz and a Varian Cary 50 spectrometer, respectively.

Results and Discussion

Sensor Device. Figure 1 shows the device (see Experimental Section) used to test the reactivity of hydrogen with various solid-state films of alkylamine- and tetraoctylammonium bromide-coated Pd, PdAg, and PdAu nanoparticles by monitoring changes in conductivity in the presence of H_2 with N_2 or air as the carrier gas. Frame A shows the device before and Frame B shows the device after drop-cast deposition of a film of octylamine ($C8NH_2$)-coated Pd MPCs. The figure also illustrates the various metal compositions (Pd, PdAg, and PdAu) and protecting ligands used in our previous work and in this study, which includes hexanethiolate (C6S), octylamine ($C8NH_2$), dodecylamine ($C12NH_2$), hexadecylamine-octadecylamine (C16-$18NH_2$), and tetraoctylammonium bromide (TOABr).

Electronic Properties of Alkylamine- and TOABr-Coated Pd Nanoparticles. Figure 2A shows cyclic voltammograms (CVs) of solid-state, drop-cast deposited films of $C8NH_2$, $C12NH_2$, C16-$18NH_2$, and TOABr-coated Pd nanoparticles. Figure 2B shows the films of $C12NH_2$ Pd, C16-$18NH_2$ Pd, and the background expanded (see dashed box in Figure 2A). The current through the film of $C8NH_2$ Pd MPCs is linear with potential, showing ohmic behavior. Current through the film of $C12NH_2$ is also ohmic but shows hysteresis because the current is close to the background (with no MPCs deposited). The CV of the film of C16−$C18NH_2$ Pd MPCs is the same as the background, indicating no conductivity through this film. The shape of the curves and the fact that the conductivity, which is proportional to the slope of the CV, decreases with increasing chainlength is consistent with an electron hopping conductivity mechanism through the films, which depends on the cluster edge-to-edge distance (exponentially), the dielectric of the

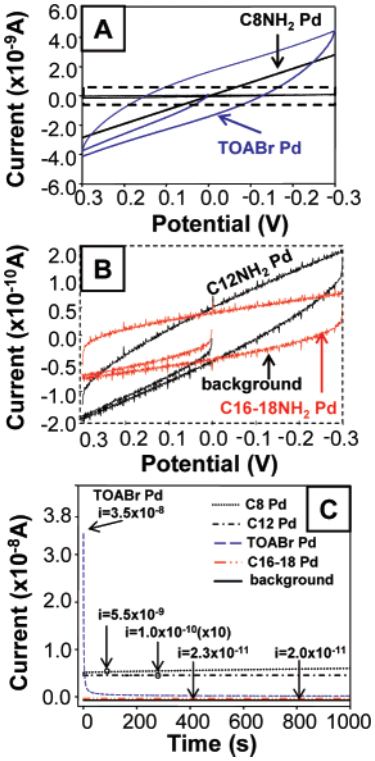

Figure 2. (A) Cyclic voltammograms (CVs) of drop-cast deposited films of $C8NH_2$, $C12NH_2$, C16-$18NH_2$, and TOABr Pd nanoparticles obtained in air from +0.3 to −0.3 V (started at 0.0 V) at a sweep rate of 100 mV/s. (B) Expanded CVs of the background (no film) and films of $C12NH_2$ Pd and C16-$18NH_2$ Pd as indicated by the dashed rectangle in (A). (C) Chronoamperometry (CA) plots of the same drop-cast films from (A) measured in air at −0.3 V for 1000 s.

medium surrounding the clusters, and cluster size.[51,53−56] Note that there is almost no current through the film of C16−18 NH_2 Pd MPCs because the cluster edge-to-edge distance is too large for significant electron hopping to occur, which is expected to be greater than 20 Å considering that the distance is estimated to be ∼1.2 times the chainlength of one ligand due to interdigitation of the monolayers from adjacent clusters.[51]

The CV of the film of TOABr-coated Pd nanoparticles is markedly different compared to that of $C8NH_2$ Pd MPCs. The current is on the same order of magnitude, but the plot does not show ohmic behavior. Instead, there is large hysteresis on the forward and reverse scan, which is consistent with the current being dominated by ions, likely due to the large excess of TOA^+ and Br^- ions in the film, since these nanoparticles could not be purified as a solid.

Figure 2C shows chronoamperometry (CA) plots in air of films of $C8NH_2$, $C12NH_2$, C16-$18NH_2$, and TOABr-coated Pd nanoparticles measured for 1000 s at −0.3 V. For the films of alkylamine-coated Pd MPCs, the current is fairly constant over time, consistent with ohmic behavior. The magnitude of current is 5.5×10^{-9}, 1.0×10^{-10}, and 2.3×10^{-11} A for films of

(53) Terrill, R. H.; Postlethwaite, T. A.; Chen, C.-h.; Poon, C.-D.; Terzis, A.; Chen, A.; Hutchison, J. E.; Clark, M. R.; Wignall, G.; Londono, J. D.; Superfine, R.; Falvo, M.; Johnson, C. S., Jr.; Samulski, E. T.; Murray, R. W. *J. Am. Chem. Soc.* **1995**, *117*, 12537−12548.
(54) Zamborini, F. P.; Leopold, M. C.; Hicks, J. F.; Kulesza, P. J.; Malik, M. A.; Murray, R. W. *J. Am. Chem. Soc.* **2002**, *124*, 8958−8964.
(55) Zamborini, F. P.; Smart, L. E.; Leopold, M. C.; Murray, R. W. *Anal. Chim. Acta* **2003**, *496*, 3−16.
(56) Ibanez, F. J.; Growrishetty, U.; Crain, M. M.; Walsh, K. M.; Zamborini, F. P. *Anal. Chem.* **2006**, *78*, 753−761.

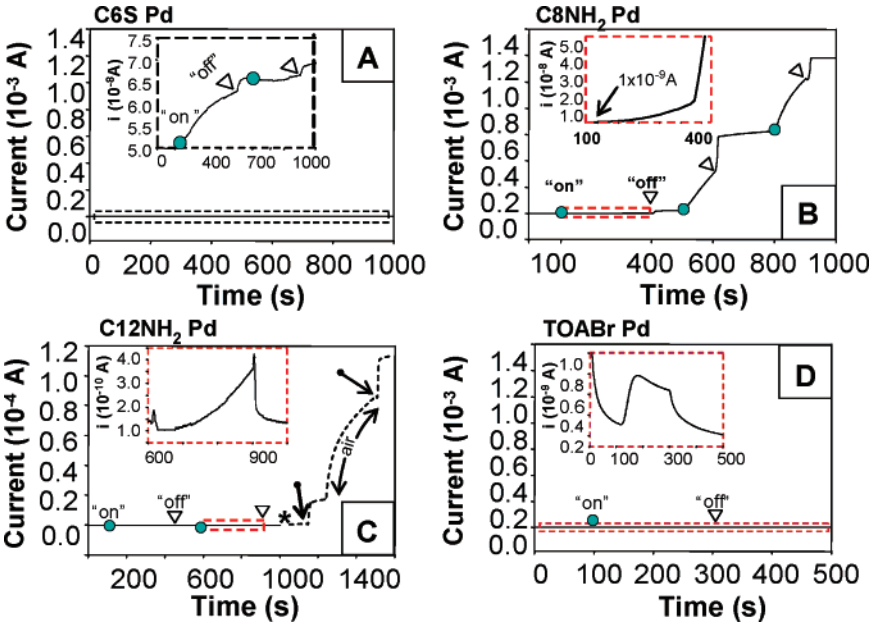

Figure 3. CA plots of films of (A) C6S Pd MPCs, (B) $C8NH_2$ Pd MPCs, (C) $C12NH_2$ Pd MPCs, and (D) TOABr Pd nanoparticles measured at −0.3 V during repeated exposure to 100% H_2 (●) and air (△) during film conditioning to reach stable currents. (Insets) Expanded plots of the regions indicated by the dashed rectangles. The arrows after the * in (C) represent exposure to 9.6% H_2.

$C8NH_2$, $C12NH_2$, and $C16\text{-}18NH_2$, respectively, showing a decrease in conductivity with increasing chainlength. The current displayed by the film of $C16\text{-}18NH_2$ Pd MPCs is again similar to the background with no MPCs deposited. The current displayed by the film of TOABr-coated Pd nanoparticles is not constant; it decreases from 3.5×10^{-8} to 2.0×10^{-10} A over 1000 s, which is consistent with a diffusion process and ionic conductivity. The final conductivity value is above the baseline, which could be due to steady-state ionic conductivity or some electron hopping through the film. In summary, the data in Figure 2 show that films of alkylamine-coated Pd MPCs conduct by an electron hopping process and those of TOABr-coated Pd nanoparticles conduct mainly by ions.

Reactivity of Films of Alkylamine- and TOABr-Coated Pd Nanoparticles to 100% H_2. Figure 3 shows CA plots of C6S, $C8NH_2$, $C12NH_2$, and TOABr Pd nanoparticles at a voltage of −0.3 V where 100% H_2 or 100% air (or N_2 for C6S) is flowing over the device at various times as indicated by H_2 "on" (●) and H_2 "off" (△), respectively. Films of $C16\text{-}18NH_2$ Pd MPCs had very little conductivity and did not change in the presence of 100% H_2 for up to 2000 s and are not shown in Figure 3. The current is stable for C6S, $C8NH_2$, and $C12NH_2$ Pd MPCs in 100% air initially as also shown in Figure 2. In the presence of 100% H_2, Figure 3A shows that the current passing through a film of C6S Pd MPCs increased irreversibly from about 5.0×10^{-8} to 7.0×10^{-8} A over a 1000 s period (see inset for expanded plot). This reflects little reactivity with H_2, which we previously determined was likely due to poisoning of the reaction between Pd and H_2 by the strongly coordinated thiolates surrounding the Pd nanoparticles.[45] Ozone- and heat-induced removal of C6S led to much greater reactivity with H_2 and reversible sensing characteristics.[45]

In contrast to C6S Pd MPCs, the conductivity of films of $C8NH_2$ and $C12NH_2$ Pd MPCs changes much more appreciably in the presence of 100% H_2 without any ozone or heat treatment. Figure 3B shows that the current through the film of $C8NH_2$ Pd MPCs increased irreversibly from about 1×10^{-9} to 5×10^{-6} A during the first 300 s of exposure (see inset), continued to rise slightly when in 100% air, and then increased to 5.0×10^{-4} A upon the second H_2 exposure. This trend continued until the film reached a final current of 1.2×10^{-3} A, which is an increase of about 6 orders of magnitude as compared to the factor of 1.4 increase for the film of C6S Pd MPCs. This shows that the more weakly coordinated octylamines do not hinder the Pd from reacting with H_2. The irreversible increase in current is likely due to restructuring of the Pd film during repeated exposure and removal from 100% H_2, which is well known for Pd materials.[1]

Figure 3C shows that the current through a film of $C12NH_2$ Pd MPCs increased from about 1×10^{-10} to about 3.5×10^{-10} A and reversibly returned close to the baseline upon the first 400 s and second 300 s (see inset) exposure to H_2. This is similar to that for films of C6S Pd MPCs, but the behavior is reversible. The * in the plot indicates that sensing was performed at this time, but the baseline was unstable and constantly increasing (vide infra). At a later time after the * (∼1150 s), the current increased to about 2×10^{-5} A and then finally to a stable value of about 1.2×10^{-4} A (the arrows in the plot after the * correspond to 9.6% H_2 exposure). The films of $C12NH_2$ Pd MPCs are overall similar to those of $C8NH_2$ Pd MPCs in that they irreversibly increase in current to a value about 6 orders of magnitude higher than the initial current, likely due to film restructuring in both cases, but the kinetics are different for the two films. Films of $C8NH_2$ Pd MPCs restructure and stabilize in a more continuous 500 s step in H_2, whereas films of $C12NH_2$ Pd MPCs initially show a somewhat stable, reversible response to H_2 that changes to a large, irreversible increase in current at times greater than 700 s in H_2. The longer time required to reach the higher current is likely due to the longer alkyl chains slowing down the reaction and film restructuring process. The final film of $C12NH_2$ Pd MPCs has a higher resistance compared to that of $C8NH_2$ Pd MPCs.

Figure 3D shows the current passing through a film of TOABr-coated Pd nanoparticles upon exposure to 100% H_2 and

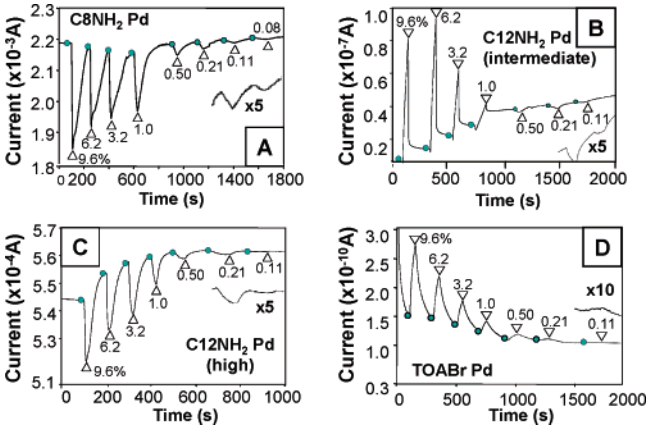

Figure 4. CA plots of films of (A) $C8NH_2$ Pd MPCs, (B) $C12NH_2$ Pd MPCs (intermediate current), (C) $C12NH_2$ Pd MPCs (high current), and (D) TOABr Pd nanoparticles exposed to H_2 concentrations from 9.6 to 0.08% as indicated in N_2 carrier gas. The films were initially exposed to 100% N_2, and the circles represent the point of exposure to the H_2 concentration indicated and open triangles represent the point of exposure back to 100% N_2.

air. These films exhibited stable, reversible increases in current in the presence of 100% H_2 immediately and did not require any conditioning (see inset). Table S.1 of the Supporting Information summarizes the results of the conditioning during initial exposure to 100% H_2 obtained on three samples of each type of film of Pd nanoparticles.

H_2 Sensing with Films of Alkylamine- and TOABr-Coated Nanoparticles. Figure 4 shows chronoamperometry (CA) plots for selected films that were exposed to H_2 concentrations from 9.6% down to 0.08% H_2. The films are initially in 100% N_2 and then exposed to various concentrations of H_2 (indicated by circles) and then back to 100% N_2 (indicated by triangles). The sensing experiments in Figure 4 occurred after conditioning the films until they were stable as discussed in Figure 3, except for those of TOABr-coated Pd nanoparticles, which did not require conditioning. Figure 4A shows that the film of $C8NH_2$ Pd MPCs exhibited a very sharp and reversible decrease in current in the presence of 9.6−1.0% H_2. The decrease in current is less pronounced below 1.0% H_2 but is noticeable for concentrations as low a 0.08% H_2 for a 100 s exposure. Figure 4B and C shows the chemiresistive response to H_2 for a film of $C12NH_2$ Pd MPCs after the first and second conditioning, respectively, as discussed in Figure 3. After the first conditioning (see the * in Figure 3C), the current through the film is on the order of 10^{-8} A and the current increases in the presence of H_2 down to 1.0%, but curiously decreases for lower H_2 concentrations down to 0.11%. The response for this film is not totally reversible as indicated by the constantly shifting baseline current to higher values. Figure 4C shows the current response of the same film after it reached a higher, more stable baseline current on the order of 10^{-4} A. The response completely changed, where the current decreased in the presence of H_2 down to concentrations of 0.11%, similar to films of $C8NH_2$ Pd MPCs. Figure 4D shows the change in current of a selected film of TOABr-coated Pd nanoparticles in the presence of H_2. The film exhibited a stable, reversible increase in current for concentrations ranging from 9.6% down to 0.11% without any pretreatment or film conditioning. There is a slight drift in the baseline over time due to a decrease in the baseline ionic conductivity with time as shown in Figure 2.

Figure 4 shows two different types of sensing behavior: those that decrease in conductivity and those that increase in conductivity in the presence of H_2. The direction depends on the baseline conductivity.[14,45] Films of $C8NH_2$ Pd and $C12NH_2$ Pd (after second conditioning) have baseline currents on the order of 10^{-3} and 10^{-4} A and decrease in current in the presence of H_2, which is consistent with what has been observed previously for well-connected, low-resistance Pd materials.[1,26] This is due to the increased resistance of the PdH_x compared to pure Pd.[29] Films of $C12NH_2$ Pd MPCs after the first conditioning have a relatively smaller baseline current on the order of 10^{-8} A, and the current increases in the presence of H_2 at concentrations greater than 1.0%. The Pd nanoparticles in these films are not well connected and the expansion in volume of the Pd when forming PdH_x leads to an overall decrease in resistance due to closer spacing or formation of connections between particles.[14] We attribute the current decrease in the presence of H_2 at concentrations of 0.50% and lower for these films to a temporary increase in resistance upon small amounts of H diffusing into α-phase Pd at low H_2 concentration.[30] Eventually, the resistance of the film should decrease once the expanded $\alpha-\beta$ or β phase Pd forms. We believe that the slow kinetics of this process at low H_2 concentration leads to the reduction in current, which would have eventually increased if exposed for longer time. Even at higher concentrations (≥1.0%), an initial drop in current occurs first, but the faster phase change kinetics eventually leads to increased current on the time scale of the exposure.[30] The increase in current for films of TOABr-coated Pd nanoparticles is not well understood. The films conduct ionically, but there may be some electron hopping as well. The expanded volume of PdH_x could affect both types of conductivity. Increased thermal motion upon H_2 adsorption into the films could also increase the current similar to that observed for films of C6S-coated Au MPCs in the presence of CO_2 gas.[57] More experiments are needed to better understand the mechanism. We also observed an increase in conductivity for TOABr-coated Au nanoparticles in the presence of H_2, but the Pd metal plays an important role since films of TOABr-coated Pd were much more sensitive, stable, and reversible.

Reactivity of Alkylamine- and TOABr-Coated PdAg and PdAu Nanoparticles to 100% H_2. We next studied the H_2 response of films of PdAg and PdAu alloy nanoparticles. These alloys are significant because Ag is cheaper than Pd, which could reduce the cost of sensors or catalysts based on these materials. From a chemical standpoint, PdAg has been shown to be more sensitive since Ag can adsorb more H into its lattice and PdAu alloys have shown faster response times due to Au hindering the $\alpha-\beta$ phase transition during H diffusion into Pd.[9−11] CVs of films of the alloy nanoparticles were very similar to those of the pure Pd and are not shown.

Figure 5A shows the change in current for a film of $C8NH_2$ PdAg when first exposed to 100% H_2. The current increased from about 1.0×10^{-10} to 1.2×10^{-8} A, which is ∼2 orders of magnitude.[58] Interestingly, this is significantly smaller than the 6 order of magnitude increase observed for $C8NH_2$ Pd films in Figure 3. The presence of less than 10% Ag in the alloy led to much higher resistance in the film following restructuring in 100% H_2. The reactivity and restructuring of these nanoparticle

(57) Choi, J.-P.; Coble, M. M.; Branham, M. R.; DeSimone, J. M.; Murray, R. W. *J. Phys. Chem. C* **2007**, *111*, 3778−3785.

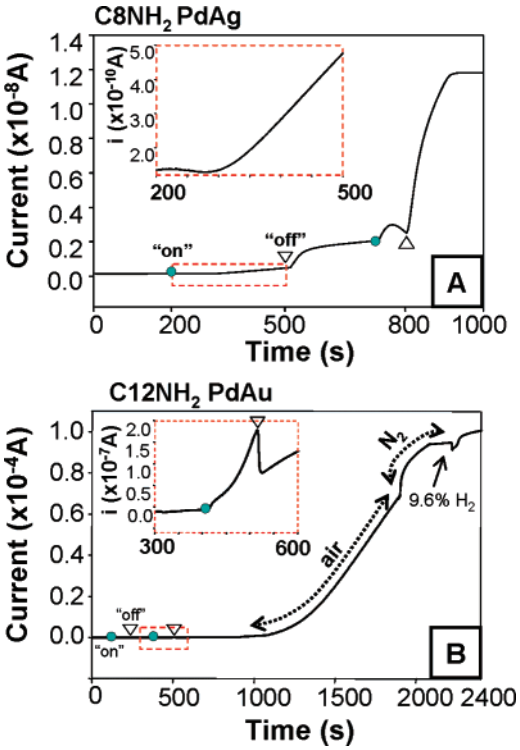

Figure 5. CA plots of films of (A) $C8NH_2$ PdAg and (B) $C12NH_2$ PdAu measured at −0.3 V during repeated exposure to 100% H_2 (●) and air (△) during film conditioning to reach stable currents. (Insets) Expanded plots of the regions indicated by the dashed rectangles.

films are clearly very sensitive to metal composition. Similarly prepared films of $C12NH_2$ PdAg films exhibited very low baseline currents and did not change significantly in the presence of 100% H_2 (data not shown). Figure 5B shows the change in current for a film of $C12NH_2$ PdAu MPCs in the presence of 100% H_2. In contrast to films of $C12NH_2$ PdAg, the $C12NH_2$ PdAu film exhibited a rapid jump in current to 10^{-7} A after about 300 s total in H_2 (first two exposures) and eventually increased to about 1.0×10^{-3} A, similar to films of $C12NH_2$ Pd MPCs. One major difference between the PdAu alloy and pure Pd, though, is that the current constantly increased in air and N_2 upon only two exposures to 100% H_2, whereas pure Pd showed some initial reversibility to H_2 during the first two exposures. As with TOABr Pd, films of TOABr PdAg nanoparticles exhibited stable, reversible increases in current immediately in the presence of H_2. Table S.2 (Supporting Information) summarizes the behavior of three different samples of Pd alloy films that were conditioned with 100% H_2 and air.

H_2 Sensing with Films of Pd Alloy Nanoparticles. Figure 6 shows the chemiresistive response to H_2 for selected alloy films following conditioning to stable currents as discussed in Figure 5. Having a low initial conductivity ($\sim 10^{-8}$ A), the current for films of $C8NH_2$ PdAg MPCs increased in the presence of H_2 concentrations from 9.6 to 0.08% (Figure 6A). This is different from films of $C8NH_2$ Pd MPCs (Figure 4A), which have a larger stable baseline current after conditioning

(58) We believe the lower initial current for $C8NH_2$ PdAg compared to $C8NH_2$ Pd is caused by a smaller amount of MPCs drop-cast deposited onto the electrode surface in this case (see Experimental Section) and irregular film deposition during drying. When preparing films of $C8NH_2$ PdAg from a more concentrated (70 mg/mL) solution, the film displayed much higher current ($\sim 1.0 \times 10^{-7}$ A) in line with the shorter alkyl chain and Ag in the alloy. Note that the differences in film thickness and initial conductivity did not change the conditioning and sensing behavior discussed next.

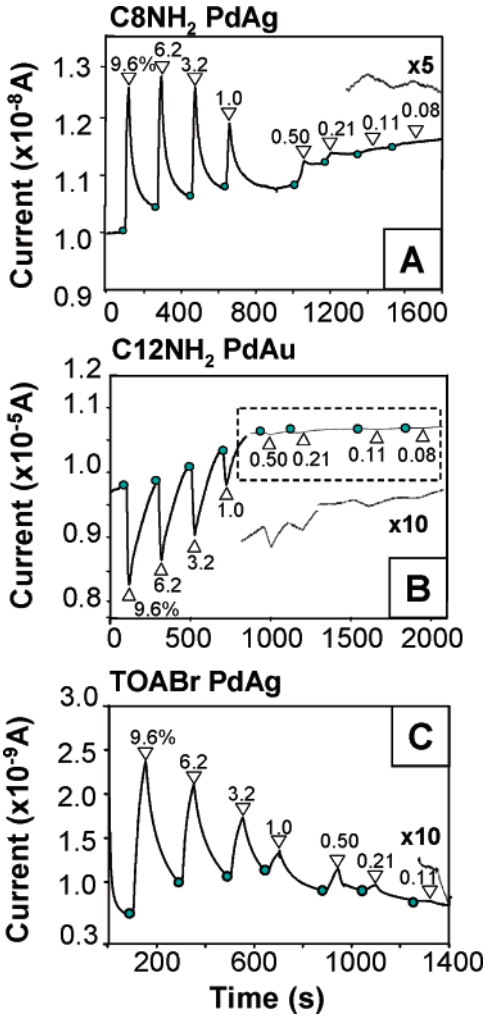

Figure 6. CA plots of films of (A) $C8NH_2$ PdAg MPCs, (B) $C12NH_2$ PdAu MPCs, and (C) TOABr PdAg nanoparticles exposed to H_2 concentrations from 9.6 to 0.08% as indicated in N_2 carrier gas. The films were initially exposed to 100% N_2, and the circles represent the point of exposure to the H_2 concentration indicated and open triangles represent the point of exposure back to 100% N_2.

(10^{-3} A) that decreased in the presence of H_2. The addition of less than 10% Ag altered the film restructuring process and H_2 sensing mechanism. Figure 6B shows the change in current for a film of $C12NH_2$ PdAu MPCs during H_2 exposure. The baseline current is on the order of 10^{-5} A and the current decreased in the presence of 9.6 to 0.08% H_2, similar to films of $C8NH_2$ Pd and $C12NH_2$ Pd after the second conditioning, but very different from films of $C12NH_2$ PdAg MPCs, which did not respond to H_2. Figure 6C shows the response for a film of TOABr PdAg nanoparticles. The current increased in the presence of 9.6 to 0.11% H_2 similar to films of TOABr Pd (Figure 4C). The baseline currents and response direction are not as sensitive to metal composition as the alkylamine-coated MPCs for the metal ratios studied. The explanation for the different types of sensing (increase or decrease in current) is the same as that described for the films of pure Pd nanoparticles.

Surface FTIR Spectroscopy Characterization. We used FTIR spectroscopy to probe the organic portion of the films before and after exposure to H_2 to gain insight into the film restructuring process and sensing mechanism. Figure 7A−D shows surface FTIR spectra for films of $C8NH_2$ Pd, $C8NH_2$

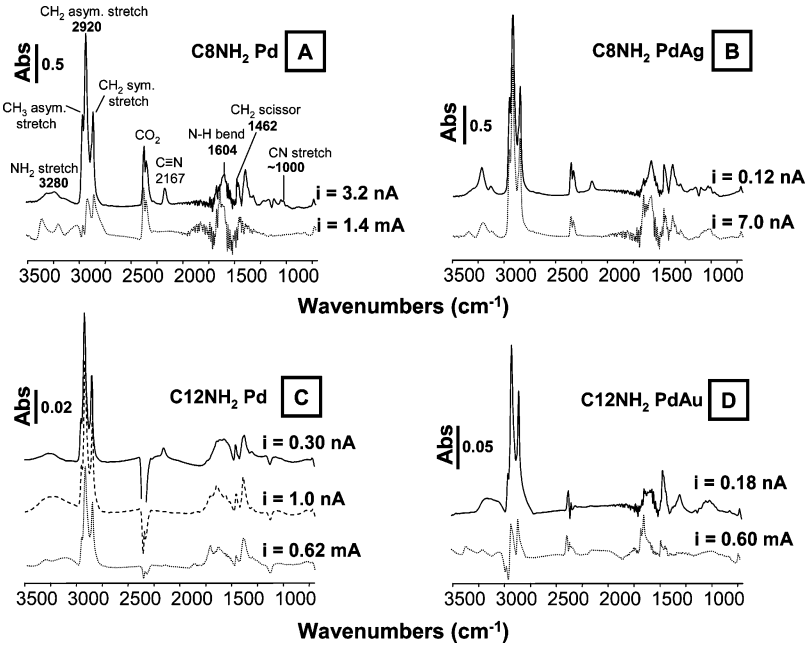

Figure 7. Surface FTIR spectra of films of (A) $C8NH_2$ Pd, (B) $C8NH_2$ PdAg, (C) $C12NH_2$ Pd, and (D) $C12NH_2$ PdAu MPCs obtained before and after exposure to 100% H_2 until they reached stable currents. Films were exposed to 100% H_2 for a total time of 500, 400, 800, and 300 s, for A−D, respectively. The number displayed next to each spectrum is the current (in amps) passing through similarly prepared films deposited onto electrodes and exposed to H_2 in parallel with the FTIR samples. The films of $C12NH_2$ Pd MPCs shows two FTIR spectra after exposure to H_2 that correspond to conditioning to intermediate current and high current.

PdAg, $C12NH_2$ Pd, and $C12NH_2$ PdAu, respectively, before[59] and after exposure to 100% H_2 that were placed in the same chamber as electrodes containing the same films for conductivity measurements. Before exposure, all of the spectra show absorbance peaks similar to those previously reported for alkylamine monolayers on Pd[60] and Au.[49] For example, the spectrum for the film of $C8NH_2$ Pd MPCs before H_2 displays peaks at 3280, 1604, and 1000 cm^{-1}, which corresponds to the N−H stretch, N−H bend, and C−N stretch, respectively, as indicated.[49] The peaks at 3000−2850 cm^{-1} are due to the asymmetric and symmetric CH_3 and CH_2 stretches, and the peak at 1462 cm^{-1} is due to a CH_2 scissor mode. In addition, we observed a sharp peak at 2167 cm^{-1}, which is in the region of a C≡N or C≡C stretching vibration. We believe this may be due to a C≡N stretch that arises from converting the R-CH_2−NH_2 to a R-C≡N by oxidation of amines catalyzed by Pd during the synthesis as reported previously for Cu(II)[61] and Pd(II)[62] complexes. The C≡N stretch for free alkyl nitriles (gas or liquid) is generally around 2230−2270 cm^{-1} and sensitive to the coordination environment.[63−66] Acetonitrile[65,67] and benzonitrile[64,65,68] adsorbed to various metal surfaces exhibited C≡N stretches between 2000 and 2250 cm^{-1}, whereas dinitriles adsorbed to Cu surfaces showed stretches in the 2080−2100 cm^{-1} range.[63,69] The C≡N stretch for isocyanides (R−N≡C) adsorbed to Pd nanoparticles[36] or Pd films[67,70,71] is 2150−2170 cm^{-1}, similar to the peak we observed, but the spectra for nanoparticles also displayed peaks at 2100−1700 and 1700−1500 cm^{-1}, assigned to a doubly bridged, and triply bridged isocyanide ligand on Pd, respectively.[36] It is difficult to envision how we could produce an isocyanide from an amine in our case. We considered the formation of R−CH═NH, but this would be expected to have a lower C═N stretch around 1600−1700 cm^{-1}.[72] Our data is most consistent with the formation of an alkyl nitrile, which has a lower stretching frequency relative to the free C≡N due to π back-bonding with the Pd metal surface.[63,69] We need to do further work to determine this peak assignment conclusively.

Figure 7A shows the FTIR spectrum of a film of $C8NH_2$ Pd MPCs before and after exposure to 100% H_2 for 500 s corresponding to currents of 3.2×10^{-9} and 1.4×10^{-3}A, respectively. There are four main changes in the spectrum following exposure to H_2 and the increase in current. First, the intensity of the CH_2 and CH_3 stretches decreased significantly. In particular, the peak height of the asymmetric CH_2 stretch decreased by 80%. Figure 3 earlier showed that the film restructures and increases in conductivity upon the first exposure to 100% H_2. The IR data show that the alkylamines are removed from the film during this process. The second change is the loss of the peak at 2167 cm^{-1}. If this peak is C≡N, then it is well known that nitriles can be reduced to amines in the presence

(59) We note that all of the spectra of these films before any H_2 exposure show very little or no changes after 4 days in ambient air.
(60) Rao, C. R. K.; Lakshminarayanan, V.; Trivedi, D. C. *Mater. Lett.* **2006**, *60*, 3169.
(61) Maeda, Y.; Nishimura, T.; Uemura, S. *Bull. Chem. Soc. Jpn.* **2003**, *76*, 2399−2403.
(62) Wang, J.-R.; Fu, Y.; Zhang, B.-B.; Cui, X.; Liu, L.; Guo, Q.-X. *Tetrahedron Lett.* **2006**, *47*, 8293−8297.
(63) Loo, B. H.; Lee, Y. G.; Frazier, D. O. *J. Phys. Chem.* **1985**, *89*, 4672−4676.
(64) Mrozek, M. F.; Wasileski, S. A.; Weaver, M. J. *J. Am. Chem. Soc.* **2001**, *123*, 12817−12825.
(65) Solomun, T.; Christmann, K.; Baumgartel, H. *J. Phys. Chem.* **1989**, *93*, 7199−7208.
(66) Storhoff, B. N.; Lewis, H. C. J. *Coord. Chem. Rev.* **1977**, *23*, 1−29.
(67) Murphy, K.; Azad, S.; Bennett, D. W.; Tysoe, W. T. *Surf. Sci.* **2000**, *467*, 1−9.
(68) Oranskaya, O. M.; Semenskaya, I. V.; Filimonov, V. N. *React. Kinet. Catal. Lett.* **1976**, *5*, 135−139.
(69) Loo, B. H.; Lee, Y. G.; Frazier, D. O. *Chem. Phys. Lett.* **1985**, *119*, 312−316.
(70) Murphy, K. L.; Tysoe, W. T.; Bennet, D. W. *Langmuir* **2004**, *20*, 1732−1738.
(71) Stapleton, J. J.; Daniel, T. A.; Uppili, S.; Cabarcos, O. M.; Naciari, J.; Shashidhar, R.; Allara, D. L. *Langmuir* **2005**, *21*, 11061−11107.
(72) Ortiz-Hernandez, I.; Williams, C. T. *Langmuir* **2007**, *23*, 3172−3178.

of Pd and H_2.[73] The third and fourth change are a sharpening and slight shift to higher wavenumber for the N−H bend around 1600 cm^{-1} and a splitting of the broad NH_2 stretch at 3280 cm^{-1} into 2 (or 3) sharper peaks. These latter differences indicate a change occurs in the coordination environment between the R−NH_2 and Pd upon exposure to H_2. This might be expected considering many of the alkylamines desorbed from the surface. This could cause orientation changes, differences in hydrogen bonding, or other interactions for the remaining alkylamines. The peak at higher wavenumbers is consistent with non-hydrogen-bonded amines as observed in dilute solutions.[74]

Figure 7B shows the FTIR spectrum of a film of $C8NH_2$ PdAg MPCs before and after exposure to 100% H_2 for 400 s corresponding to currents of 1.2×10^{-10} and 7.0×10^{-9}A, respectively. The spectrum has some small differences compared to the film of $C8NH_2$ Pd MPCs before exposure to H_2. First, the peak attributed to nitriles at 2167 cm^{-1} is much smaller in intensity and there are two sharp peaks in the NH_2 stretching region as opposed to one broad peak. Adding less than 10% Ag to the reaction clearly reduced the formation of nitriles and changed the coordination environment of the amines. This suggests that many of the Ag atoms reside at the surface of the nanoparticles.[75] After exposure to H_2, the spectrum is drastically different compared to pure Pd. Most notably, the intensity of the CH_2 and CH_3 stretches barely decreased (only 4% for the asymmetric CH_2 stretch) and there is a new peak that appears near 1700 cm^{-1}. Similar to pure Pd, the nitrile peak disappeared and a better defined third peak appeared at higher wavenumbers in the NH_2 stretching region. This peak is lowest in intensity out of the three peaks for the film of PdAg MPCs, but is largest in intensity for the Pd MPCs.

Figure 7C shows the FTIR spectrum of a film of $C12NH_2$ Pd MPCs before H_2, after the first conditioning (800 s in 100% H_2), and after the second conditioning until the film reached stability. The corresponding currents are 3.0×10^{-10}, 1.0×10^{-9}, and 6.2×10^{-4} A, respectively. The spectrum before H_2 exposure is very similar to that of the film of $C8NH_2$ Pd MPCs, where the NH_2 stretch is broad and there is a noticeable absorbance band attributed to nitriles. After the first conditioning, there is a small 12% decrease in the asymmetric CH_2 stretch and after the second, there is a 36% loss of this peak. The NH_2 peaks remained fairly broad with the presence of a small broad peak appearing around 3313 cm^{-1}, instead of splitting into three sharp peaks as observed for films of $C8NH_2$ Pd. Another similarity to films of $C8NH_2$ Pd MPCs is that the nitrile peak disappeared after the first conditioning.

Figure 7D shows the FTIR spectrum of a film of $C12NH_2$ PdAu MPCs before and after conditioning with 100% H_2 for 300 s, corresponding to currents of 1.8×10^{-10} and 6.0×10^{-4} A, respectively. The spectrum before H_2 is similar to the film of $C12NH_2$ Pd MPCs, except that there is no evident peak for the nitrile at 2167 cm^{-1}. As with Ag, this shows that the presence of less than 10% Au affected the formation of nitriles. There are also small differences in the NH_2 stretching and bending region. After exposure to H_2, the spectrum is very similar to that of $C8NH_2$ Pd films. The asymmetric CH_2 stretched decreased by ∼62% and the initially broad peak for the NH_2 stretch split into three sharper peaks.

Taken together with the current data, Figure 7 shows a strong correlation between monolayer desorption and change in film conductivity during the first exposure to 100% H_2. Films of $C8NH_2$ Pd MPCs, $C12NH_2$ PdAu MPCs, and $C12NH_2$ Pd (second conditioning) increased in conductivity by 5−6 orders of magnitude after a 500, 300, and >800 s exposure, respectively, and showed a correspondingly large loss of the alkylamine monolayer in the IR spectra (80, 62, and 36%, respectively). In addition, the nitriles were reduced to amines (for pure Pd) and the coordination environment of the NH_2 groups was altered. This shows that monolayer desorption and coordination changes accompany film restructuring and conductivity increases. Films of $C8NH_2$ PdAg and $C12NH_2$ Pd MPCs (first conditioning) showed a much smaller 1−2 order of magnitude conductivity change after 400 and 800 s, respectively, and a correspondingly much smaller loss of alkylamines from the surface (4 and 12%, respectively). Small changes in the spectrum include loss of the nitrile peak and changes in the NH_2 stretch. The IR and conductivity data show that for pure Pd, the longer $C12NH_2$ monolayer enhances stability and reduces the reactivity to 100% H_2. The presence of less than 10% Ag enhanced stability of the monolayer and reduced the amount of film restructuring for $C8NH_2$-coated MPCs compared to pure Pd whereas the presence of less than 10% Au reduced monolayer stability and increased the restructuring for $C12NH_2$-coated MPCs compared to pure Pd. This may be due to stronger bonding between alkylamines and PdAg as compared to alkylamines and PdAu.

Atomic Force and Optical Microscopy Characterization. We used optical microscopy and AFM to directly image various films before and after exposure to 100% H_2 to determine if morphological changes occur during the film conditioning/restructuring process. Figure 8A shows an optical image and Figure 8B shows the corresponding AFM image in the same area as indicated by the dashed box of a film of $C8NH_2$ Pd MPCs deposited on an electrode device before exposure to H_2. Figure 8C and D shows the optical and corresponding AFM image, respectively, of the same area after exposure to 100% H_2 for 500 s, compressed air for 200 s, and ambient air for 5 min during the AFM setup. The optical image shows a change in the morphology with the appearance of several black features in the image. The corresponding AFM image shows that these are ∼100 nm tall raised features (or islands) that form on the surface. The arrows in Figure 8D show the same area on the surface as in Figure 8B. Morphological changes upon incorporation of H into Pd and subsequent removal are well known to occur.[1] The morphological changes observed by microscopy are consistent with the 5−6 order of magnitude conductivity increase and 80% loss of $C8NH_2$ ligands from the MPCs observed from CA plots and surface FTIR data, respectively. In addition, powder X-ray diffraction (XRD) data on $C8NH_2$ Pd MPCs show that the domain size of the particles increases from 2.4 to 12.8 nm after 100% H_2 exposure as determined by the peak width of the Pd(111) peak and the Scherrer equation (Figure S.1, Supporting Information). This is consistent with the morphological changes observed with AFM and optical images. Figure 8E and F show optical and AFM images,

(73) Sachtler, W. M. H.; Huang, Y. *Appl. Catal. A* **1999**, *182*, 365−378.
(74) Pavia, D. L.; Lampman, G. M.; Kriz, G. S. *Introduction to Spectroscopy*; Harcout Brace College: New York, 1996.
(75) Hostetler, M. J.; Zhong, C.-J.; Yen, B. K. H.; J, A.; Gross, S. M.; Evans, N. D.; Porter, M.; Murray, R. W. *J. Am. Chem. Soc.* **1998**, *120*, 9396−9397.

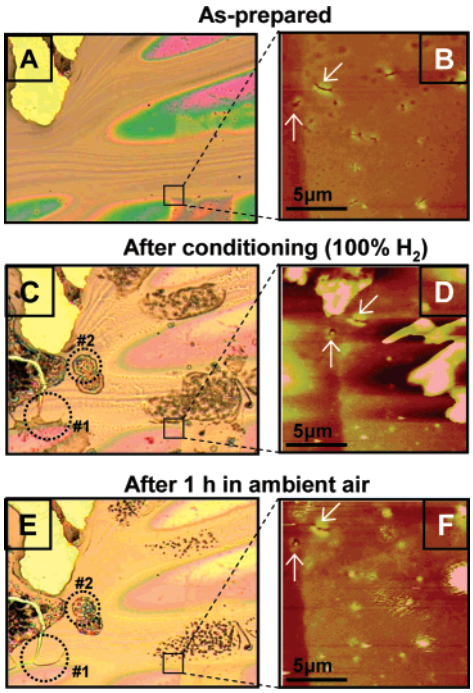

Figure 8. Optical (A, C, E) and AFM (B, D, F) images of a film of $C8NH_2$ Pd MPCs before (A, B) and after (C, D) conditioning by exposure to 100% H_2 for 500 s and air for 200 s. (E, F) shows the same film after an additional 1 h exposure to air. Circles labeled #1 represent areas were the film healed, and circles labeled #2 represent areas where the films changed irreversibly after exposure to 1 h in air.

respectively, of the same area of the same surface after another 1 h of exposure to ambient air. Several of the black features in the optical image and bright features in the AFM image disappeared, showing that there are slow morphological changes that occur over longer periods of time after exposure to H_2. Many of the regions appear to heal themselves as indicated by the circle marked #1, but several regions were also altered irreversibly as indicated by the circle marked #2 (Figure 8C and E).

To directly correlate morphology changes with changes in current and the FTIR data, we drop-cast deposited films of $C8NH_2$ Pd, $C12NH_2$ Pd, $C8NH_2$ PdAg, and $C12NH_2$ PdAu MPCs onto electrodes and obtained optical and AFM images along with current data before and after conditioning with 100% H_2. Figure S.2 of the Supporting Information shows the results. In general, films of $C8NH_2$ Pd and $C12NH_2$ PdAu MPCs showed the largest morphology changes, which is consistent with the 5−6 order increase in current and large loss of alkylamine monolayer. Films of $C12NH_2$ Pd and $C8NH_2$ PdAg showed very small morphology changes, consistent with the smaller loss of monolayer in the FTIR and smaller increase in current for the $C8NH_2$ PdAg MPC film. Films of $C12NH_2$ Pd exhibit a large 5−6 order of magnitude increase in current, but the slower kinetics of this process may lead to smaller morphological changes in the film. Powder XRD data obtained on these films are also consistent with the conductivity, FTIR, and microscopy data (Figure S.1, Supporting Information).

Sensor Comparisons. The analytical signal used for the detection of H_2 is % response as described by the following equation:

$$\%\ \text{response} = (i_r - i_b)/i_b \times 100\% = \Delta i/i_b \times 100\%$$

where i_b is the initial baseline current in 100% N_2, i_r is the current in the presence of H_2/N_2 mixture, and $\Delta i = (i_r - i_b)$. A negative value is equal to a decrease in the current upon exposure to H_2 and vice-versa. Figure 9 shows the average calibration curves plotting the % response (y-axis) versus the H_2 concentration (x-axis) for the six tested films. The points and curves represent the average of three samples. Figure 9A and C shows the response of films whose conductivity increased in the presence of H_2 from 0.0 to 0.50% and from 0.0 to 9.6% H_2, respectively. Figure 9B and D shows the response of films whose conductivity decreased in the presence of H_2 from 0.0 to 0.50% and from 0.0 to 9.6% H_2, respectively. All the films displayed fairly linear behavior below 0.50% H_2 (not forced through the origin). The behavior from 0.0 to 9.6% H_2 depended upon the stabilizer surrounding the particles. Films of alkylamine-coated MPCs exhibited nonlinear behavior above 0.50% due to the $\alpha-\beta$ phase transition, which occurs anywhere from 0.3[7] to 2.0%[1,2] H_2, and saturation of H in Pd at higher concentrations. Films of TOABr-stabilized nanoparticles were also nonlinear but did not reach saturation up to 9.6%. The slopes in Figure 9A reflect the following sensitivity order for films that increase in current: TOABr Pd (22.4) > TOABr PdAg (18.8) > $C8NH_2$ PdAg (6.6). The slopes in Figure 9B reflect the following sensitivity order for films that decrease in current: $C12NH_2$ Pd (at intermediate current) (−10.5) > $C12NH_2$ PdAu (−4.9) > $C8NH_2$ Pd (−2.9) > $C12NH_2$ Pd (at high current) (−0.8). All of the films easily detect H_2 below the explosive limit. Films of $C8NH_2$ Pd and PdAg MPCs exhibited the lowest detection limit (0.08%), whereas films of $C12NH_2$ PdAu and $C8NH_2$ PdAg displayed the fastest response times of 10−15 and 10−20 s, respectively. Others have shown that PdAu and PdAg alloy films show faster response times and greater sensitivity, respectively.[9−11] This is consistent with the fast conditioning and response of $C12NH_2$ PdAu MPC films. However, it is important to note that the film thickness (or nanoparticle loading) is not constant for these films, which could also affect the response and recovery times due to different diffusion lengths for H into the film. Films of PdAu alloys described in the literature[11] were less sensitive to H_2; however, our films of $C12NH_2$ PdAu MPCs were more sensitive compared to those of $C12NH_2$ Pd MPCs at high current. We were unable to directly compare films of $C8NH_2$ Pd with $C8NH_2$ PdAg since they have different sensing mechanisms. The response of films of TOABr PdAg were similar to those of TOABr Pd at 0.50% and below but 2−3 times higher at 1.0% and above. Table 1 displays the response direction, limit of detection, % response measured at 1% H_2, and range of response times for 3 different samples of each type of the 6 films studied. Table S.3 of the Supporting Information shows all of the data for each sample measured, including averages and standard deviations.

Conclusions

We prepared and studied the H_2 reactivity of drop-cast films of chemically synthesized alkylamine−coated Pd, PdAg (10:1) and PdAu (10:1) MPCs and films of tetraoctylammonium bromide (TOABr)-stabilized Pd and PdAg (10:1) nanoparticles. The as-prepared films are highly reactive to H_2 and do not require O_3 or thermal treatment as previously observed for films of C6S-coated Pd MPCs. The films can be placed into two categories: those that decrease in current in the presence of H_2

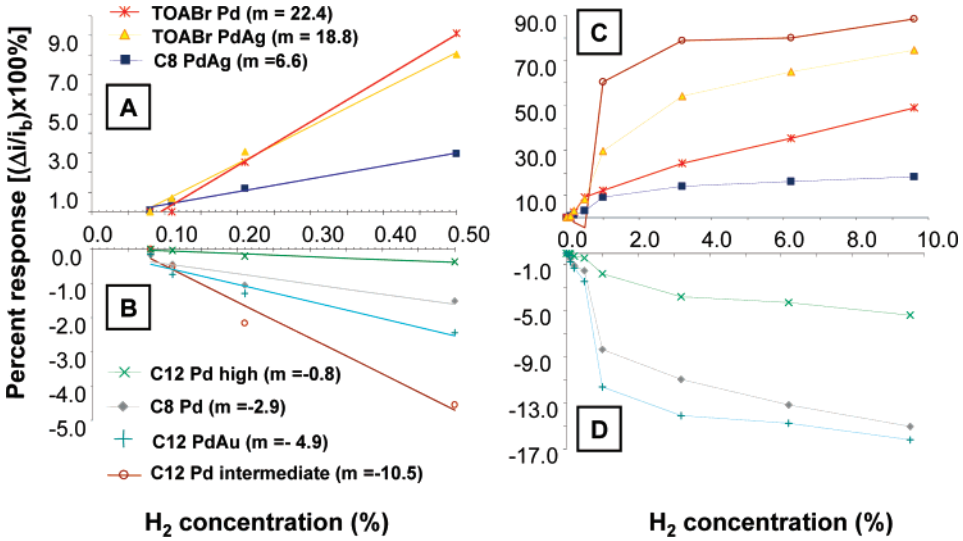

Figure 9. Calibration curves showing the percent response versus H_2 concentration from 0.00 to 0.50% (A, B) and 0.0 to 9.6% (C, D) for each sensor described in this study. The sensors are divided into those that increase in current in the presence of H_2 with positive slopes (A, C) and those that decrease in the presence of H_2 with negative slopes (B, D). The points on the curves represent the average percent response from three sensor devices at each H_2 concentration. The linear regression fits in (A, B) are not forced through the origin and the lines in (C, D) are present as a guide to the eye.

Table 1. Sensing Characteristics of the Six Tested Films

type of sensor response direction = increase in current	limit of detection (% H_2)			percent response at 1.0% H_2			response time at 1.0% H_2 (s)[a]
	S#1	S#2	S#3	S#1	S#2	S#3	
TOABr Pd	0.21	0.21	0.21	13.0	9.2	13.9	40−55
TOABr PdAg	0.11	0.11	0.11	32.5	28.9	27.1	60−70
C_8NH_2 PdAg	0.11	0.08	0.11	6.9	9.6	10.5	10−20
$C_{12}NH_2$ Pd (medium current)	0.11	0.11	0.11	69.2	44.5	67.7	50−90
type of sensor response direction = decrease in current	**limit of detection (% H_2)**			**percent response at 1.0% H_2**			**response time at 1.0% H_2 (s)[a]**
	S#1	S#2	S#3	S#1	S#2	S#3	
C_8NH_2 Pd	0.08	0.08	0.08	−8.8	−10.0	−4.3	20−30
$C_{12}NH_2$ Pd (high current)	0.11	0.11	0.11	−1.8	−1.9	−3.2	10−20
$C_{12}NH_2$ PdAu	0.08	0.08	0.08	−7.0	−11.6	−14.7	10−15

[a] Note that the film thickness (or nanoparticle loading) is not constant for these films. This could have an affect on the response time due to different lengths for H diffusion into the films.

and those that increase. Films of $C8NH_2$ Pd, $C12NH_2$ Pd (second conditioning), and $C12NH_2$ PdAu exhibit large 5−6 order of magnitude irreversible increases in current upon the first exposure to 100% H_2, which is accompanied by a large loss of the alkylamine monolayer and noticeable morphological changes in the case of $C8NH_2$ and $C12NH_2$ PdAu films. After this irreversible conditioning/restructuring, the films exhibit stable, reversible decreases in current in the presence of H_2 concentrations down to 0.08%. Films of $C12NH_2$ Pd (first conditioning) and $C8NH_2$ PdAg exhibit a much smaller 1−2 order of magnitude irreversible increase in current upon the first exposure to 100% H_2, which is accompanied by very little loss of the alkylamine monolayer and correspondingly small morphological changes in the film. Afterward, the films exhibit reversible increases in current in the presence of H_2 concentrations down to 0.08%, which is stable only for the case of PdAg MPCs. Films comprised of TOABr-coated Pd and PdAg exhibit reversible, stable increases in current in the presence of H_2 concentrations down to 0.11% without any pretreatment or conditioning. Alkylamine-coated Pd MPCs change in current through higher resistance of PdH_x or lower resistance during volume increases of PdH_x; however, the sensing mechanism of ionically conductive TOABr-coated Pd nanoparticles is less understood. All of the films are easy to synthesize on a large scale, and the devices are simple to construct, leading to responses to H_2 well below the explosive limit. For sensing, films of TOABr-coated Pd and PdAg alloy nanoparticles are the most promising of all the films because of their high sensitivity, wider detection range, and no need for pretreatment or conditioning. Out of the films of alkylamine-coated MPCs, those of $C8NH_2$ PdAg MPCs are the best because they exhibit the highest sensitivity, lowest limit of detection, are the most stable, have fast response, and require very little conditioning in 100% H_2 to reach stable, sensing behavior. They would also be slightly lower in cost due to the incorporation of Ag into the material, which is cheaper than Pd. $C12NH_2$ PdAu films were fairly sensitive and demonstrated the fastest response with H_2 during the conditioning process and sensing. Catalysis applications for these materials need further exploration.

Acknowledgment. We gratefully acknowledge the National Science Foundation (CHE-0518561) and the Kentucky Science

and Engineering Foundation for partial support of this research. We also acknowledge Andres J. Puppato from the Department of Chemistry at the University of Louisville for providing valuable help in the use of NMR. We thank Kevin M. Walsh, Mark M. Crain, and Ana Sanchez from the Department of Electrical and Computer Engineering at the University of Louisville for use of the clean room to microfabricate the electrode devices.

Supporting Information Available: Tables showing the conditioning data for films of pure Pd nanoparticles and Pd alloy nanoparticles, powder X-ray Diffraction data, optical and AFM images of the alkylamine-coated Pd and Pd alloy films before and after conditioning with H_2, and table showing the sensor response data for each sample used in this study (including average response, standard deviation, relative standard deviation, and percent success for detecting a specific H_2 concentration for each film). This information is available free of charge via the Internet at http://pubs.acs.org

JA076000H